inorganics

MDPI

Article

Synthesis, Characterization, and Cytotoxicity Research of Sulfur-Containing Metal Complexes

Yanting Yang, Danqin Li and Mei Luo *

Department of Chemistry and Chemical Engineering, Hefei University of Technology, Hefei 230002, China; yangyanting0626@163.com (Y.Y.); 18325610866@163.com (D.L.)
* Correspondence: luomei@pku.edu.cn

Abstract: In this experiment, the excellent coordination ability of sulfur-containing ligands was utilized. Diphenylacetyl disulfide and 3,3′-diaminodiphenyl sulfone were selected as ligands, and $Cu(NO_3)_2{\cdot}3H_2O$, $Ni(NO_3)_2{\cdot}6H_2O$ and $ZnCl_2$ were reacted under one-pot conditions to synthesize three mononuclear complexes: $[C_4H_{18}CuO_{12}S_2]$(I), $[C_{12}H_{18}N_4NiO_{11}S]$(II) and $[C_{24}H_{24}Cl_2N_4O_4S_2Zn]$(III). Complex (I) belongs to the orthorhombic crystal system with space group Pbca, while complexes (II) and (III) belong to the monoclinic crystal system with space groups P21/n and P2/n. The crystal structure of the complex was determined using X-ray diffraction (XRD). The structure of the complex was analyzed using infrared Fourier transform infrared spectroscopy (FT-IR), ultraviolet–visible spectroscopy (UV–Vis), nuclear magnetic resonance (NMR), and electrospray mass spectrometry (ESI-MS), and the thermal stability and composition of the complex were detected via thermogravimetry (TGA). In terms of application, the biological activity of complexes (I)–(III) in human cancer cell lines (lung cancer A549, liver cancer SMMC-7721, breast cancer MDA-MB-231, and colon cancer SW480) was tested using the MTS method. The results showed that complex (II) had a good inhibitory effect on breast cancer MDA-MB-231.

Keywords: one-pot method; complex; crystal structure; cytotoxicity

check for updates

Academic Editor: Dušan Dimić

Received: 17 December 2024
Revised: 7 January 2025
Accepted: 13 January 2025
Published: 17 January 2025

Citation: Yang, Y.; Li, D.; Luo, M. Synthesis, Characterization, and Cytotoxicity Research of Sulfur-Containing Metal Complexes. *Inorganics* **2025**, *13*, 26. https://doi.org/10.3390/inorganics13010026

Copyright: © 2025 by the authors. Licensee MDPI, Basel, Switzerland. This article is an open access article distributed under the terms and conditions of the Creative Commons Attribution (CC BY) license (https://creativecommons.org/licenses/by/4.0/).

1. Introduction

Metal–organic complexes are a type of compound formed by coordination bonds between metals and organic ligands [1]. They can be used to synthesize novel metal–organic complexes with different structures and functions through the selection of metal centers and ligands [2–4], and accordingly, they are widely used in fields such as catalysis [5], materials [6], drug design [7], and sensing technology [8]. Organosulfur metal complexes represent an important branch of metal–organic complexes and are characterized using sulfur-containing compounds as ligands to form stable coordination bonds with metal centers. Sulfur-containing compounds are an excellent class of ligands with multiple coordination modes (such as monodentate, bidentate, and bridging) [9], playing an important role in the synthesis of metal–organic complexes. Organic sulfur compounds are abundant in sources and exist in many plants in nature, with special chemical properties and biological activities [10–12]. Studies have shown that organic sulfur compounds can affect the expression of related proteins in cancer cells, thereby inhibiting their proliferation. This finding also proves that organic sulfur compounds have the potential to become anticancer drugs [13–16]. Some achievements have recently been made in the treatment of cancer with sulfur-containing compounds. In 2018, Soltani et al. [17] isolated five new sulfur-containing

compounds from the broad-leaved Aweigen and conducted cytotoxicity experiments on the human cancer cell lines A2780, A549, HeLa, and HCT116. Some sulfur-containing compounds have moderate cytotoxicity [17]. In 2019, Balakrishnan et al. [18] synthesized two complex crystals by directly reacting potassium morpholine dithiocarbamate ($K^+C_5H_8NOS_2$) ligands with nickel and copper metals and studied the inhibitory effects of the two complexes on Gram-positive and Gram-negative bacteria. The experimental results revealed that the synthesized complexes had good antibacterial activity [18]. In 2020, Yekke-Ghasemi et al. [19] successfully synthesized three dithiocarbamate metal complexes and tested their cytotoxicity against HeLa and MCF-7 cancer cell lines. The results showed that the three novel complexes were more cytotoxic than cisplatin [19]. In 2023, Singh et al. [20] successfully prepared 2-((2-(benzylthio) phenyl) imino) methyl)-4-chlorophenol cobalt, nickel, copper, and zinc metal complexes, and the zinc complexes showed excellent anti-inflammatory and antidiabetic activities. In 2024, Czylkowska et al. [21] synthesized a series of metal complexes using 5-(1-methylpyrrole-2-yl) methyl)-4-(2-chlorophenyl)-1,2,4-triazoline-3-thione ligands. Under in vitro conditions, the metal complexes showed good cytotoxicity against A549 and HT-29 cancer cell lines, with the Cu(II) complex having the highest activity (IC_{50} = 247.90 ± 2.30) [21]. Although many studies have been conducted on organic sulfur metal complexes, there is still much research space. In this work, two sulfur-containing ligands, namely, bis(phenylacetyl) disulfide and 3,3-diaminodiphenyl sulfone, were used to synthesize several novel metal complexes with metal salts under heating conditions using a one-pot method [22,23]. Their structures were characterized using the EA, XRD, FT-IR, UV–Vis, NMR, ESI-MS and TGA methods. The cytotoxicity of the complexes was preliminarily screened via the MTS method.

2. Results and Discussion

2.1. Crystal Structure Analyses of Complexes (I)–(III)

The Figure 1 shows the crystal structures of complexes (I)–(III) and S_8. Complexes (I) (Figure 1a) and S_8 (Figure 1b) have an orthorhombic crystal system with space groups Pbca and Fddd, respectively, whereas complexes (II) (Figure 1c) and (III) (Figure 1d) are both monoclinic with space groups $P2_1/n$ and P2/n, respectively.

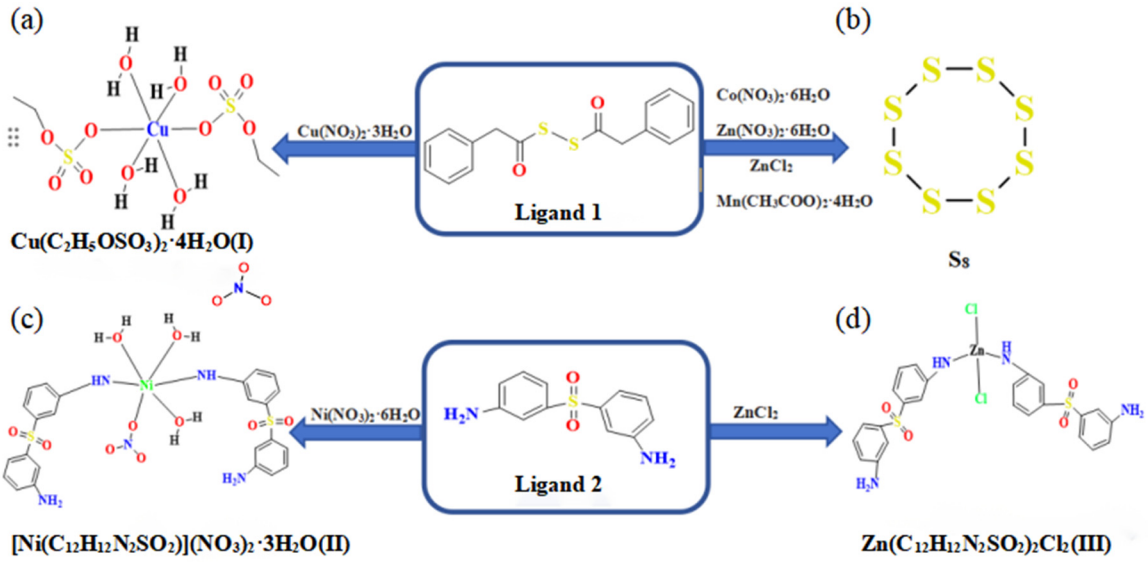


Figure 1. Synthesis protocol of complexes (I)–(III). (**a**) for (I), (**b**) for S_8, (**c**) for (II) and (**d**) for (III).

Complex (I) is not formed by direct chelation of metal ions and ligands but by ligand bond cleavage and recombination followed by coordination with metal salts; this may be

due to the breaking of S–S bonds under the effect of Lewis acids, which further react with oxygen atoms in air and ethoxy groups in ethanol to form complexes similar to copper sulfate salts. The metal center Cu^{2+} of complex (I) is coordinated via six coordination units and has two symmetrical structural units. Metal Cu(II) is connected to six oxygen atoms, forming a slightly distorted octahedral configuration, where two O atoms (O1, $O1^{i}$) are derived from O in the ethyl sulfate group, and the other four O atoms (O5, $O5^{i}$, O6, $O6^{i}$) originate from four H_2O molecules. The longest bond length between Cu1-O1 and Cu1-$O1^{i}$ is 2.4052 (12) Å, whereas the shortest bond length between Cu1-O5 and Cu1-$O5^{i}$ is 1.9520 (9) Å. The cis angle and trans angle around the Cu1 atom are 97.15 (13)° and 150.61 (12)°, respectively. Molecules form hydrogen bonds within and between molecules through the O atoms on sulfate ions and the H atoms on water molecules, ultimately forming a three-dimensional network structure. The crystal stacking diagram is shown in the Figure 2. The S_8 crystal is a "crown-shaped" structure formed by eight S atoms, which are divided into upper and lower layers. The bond angles of the S–S bonds are all approximately 108°. The structure of the S_8 crystal has already been reported in great detail and will not be repeated here.

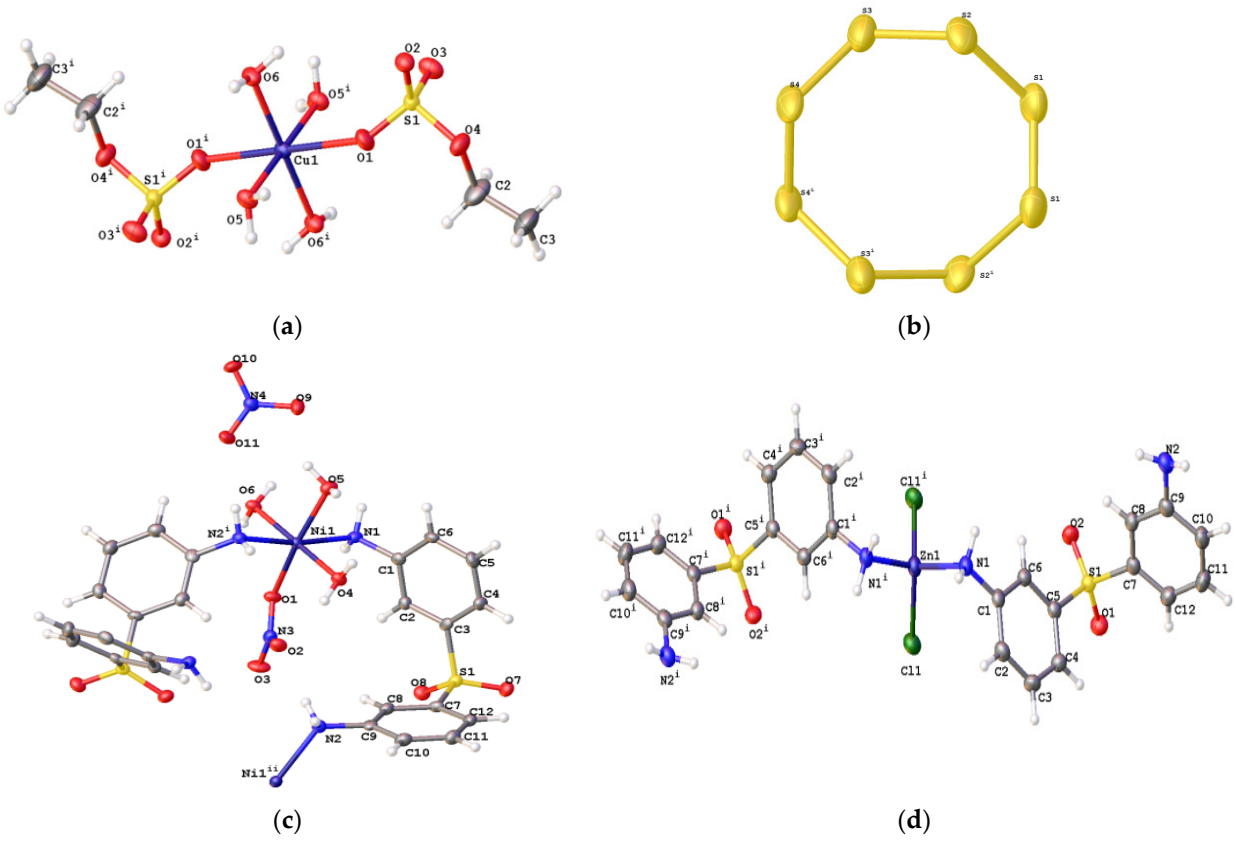


Figure 2. ORTEP molecular structures of complexes, (**a**) for (I), (**b**) for S_8, (**c**) for (II) and (**d**) for (III), with a 30% thermal ellipsoid probability.

Complex (II) is a twisted octahedral configuration centered on Ni(II), with a coordination number of six. The mononuclear crystal complex (II) contains one 3,3′-diaminodiphenyl sulfone ligand, three water molecules, and two NO_3^- ions (one of which is in a free state). From the crystal structure diagram below, it can be observed that the two molecules are bridged to Ni(II) through the N atom on the ligand NH_2. Molecules also communicate with each other through C(8)-H(8···O(2)#1, N(1)-H(1A)···O(9)#3, O(4)-H(4A)···O(3)#2, and other hydrogen bonds (see Table 1), which are stacked together and connected along the b-axis direction to form a three-dimensional chain structure.

Table 1. Partial hydrogen bond data for complexes (I)–(III).

	D-H···A	d(D-H)/Å	d(H···A)/Å	d(D···A)/Å	∠(DHA)/°
Complex (I)	O(5)-H(5B)···O(2)#2	0.87	1.91	2.7145(14)	152.6
	O(6)-H(6B)···O(3)#4	0.87	1.92	2.7392(15)	156.5
Complex (II)	C(8)-H(8)···O(2)#1	0.95	2.55	3.144(7)	120.9
	N(1)-H(1A)···O(9)#3	0.91	2.16	3.048(7)	166.5
	O(4)-H(4A)···O(3)#2	0.87	2.13	2.926(6)	152.4
Complex (III)	N(1)-H(1A)···N(2)#2	0.91	2.12	3.025(3)	176.0
	N(2)-H(2A)···O(2)#3	0.88	2.27	3.068(2)	150.4
	N(1)-H(1B)···Cl(1)#4	0.91	2.57	3.4355(18)	159.2
	C(2)-H(2)···Cl(1)#4	0.95	3.22	3.986(2)	139.3
	C(3)-H(3)···O(1)#5	0.95	2.66	3.254(3)	121.5
	C(6)-H(6)···N(2)#2	0.95	3.05	3.630(3)	120.5

Complex (III) is a slightly distorted tetrahedral configuration formed by the 4-coordination of Zn(II). The central ion Zn^{2+} is directly connected to two Cl^- and two N donors (N1, $N1^i$) on 3,3′-diaminodiphenyl sulfone ligands, with main bond lengths and bond angles of $d_{N1\text{-}Zn1} = d_{N1^i\text{-}Zn1} = 2.0530$ (17) Å and $d_{Cl1\text{-}Zn1} = d_{Cl1^i\text{-}Zn1} = 2.2393$ (6) Å, respectively, and ∠N1-Zn1-$Cl1^i$ = 112.36(5)°, ∠Cl1-Zn1-$Cl1^i$ = 109.43(3)°, and ∠N1-Zn1-$N1^i$ = 105.00(9)°. Molecules interact with each other through four types of hydrogen bonds, namely, N-H···N, N-H···O, C-H···N, and C-H···O, forming a regular three-dimensional network structure.

2.2. IR Analyses of Complexes (I)–(III)

Figure 3 shows all the infrared absorption peaks of complexes (I)–(III) in the range of 4000–500 cm^{-1}. The stretching vibration absorption peak of OH in water molecules is located at 3491 cm^{-1}, whereas the absorption peak of free OH is generally at approximately 3700–3500 cm^{-1} [24]. However, due to the presence of intramolecular and intermolecular hydrogen bonds in complex (I) molecules (see Table 1), the absorption peak redshifts [25]. In the figure, two absorption peaks were observed at 2990 cm^{-1} and 2899 cm^{-1}, indicating the presence of both CH_3 and CH_2 in the molecular structure of complex (I). The in-plane bending vibration absorption peak of C-H on the methyl group was observed at 1380 cm^{-1}, and the stretching vibration frequency of the C–C bond on the alkyl group was observed near 1235 cm^{-1}. There are two characteristic absorption peaks of sulfate ions: one peak, located at 1200–1000 cm^{-1}, is the symmetric stretching vibration peak of sulfate ions [26], which is commonly used to determine whether sulfate ions are present in the molecule, and the other peak, located near 1300–1100 cm^{-1}, is the asymmetric stretching vibration peak of sulfate ions. The corresponding absorption peaks in the figure are at 1065 cm^{-1} and 1020 cm^{-1}.

Complexes (II) and (III) are two types of complex crystals synthesized from the same ligand with different metal salts. They share certain similarities in composition and structure, which are particularly evident in infrared images. We observe that complex (III) has two distinct absorption peaks at 3585 cm^{-1} and 3515 cm^{-1}, corresponding to the stretching vibration peaks of NH_2 [25], whereas complex (II) has only one absorption peak at 3512 cm^{-1}; this may be due to the simultaneous presence of -OH and -NH_2 groups in complex (II) and the similar range of their characteristic infrared absorption peaks. Therefore, the absorption peaks of the two may partially overlap, resulting in only one absorption peak of a primary amine being visible from the graph. Figure 3 shows that complex (II) indeed has a broad peak at 3400 cm^{-1}, which is consistent with the characteristic absorption of OH. Both complexes (II) and (III) have benzene ring structures, and the benzene ring generally has several characteristic absorption peaks. First, there are

three weak absorption peaks at 3100–3000 cm^{-1}, which are caused by the C-H stretching vibration of the benzene ring. In the figure, they are specifically shown as complexes (II) (3180 cm^{-1}, 3095 cm^{-1}, and 2925 cm^{-1}) and (III) (3130 cm^{-1}, 3065 cm^{-1}, and 3010 cm^{-1}). Second, complexes (II) and (III) have two strong infrared absorption peaks at 1600 cm^{-1} and 1435 cm^{-1} and 1605 cm^{-1} and 1480 cm^{-1}, respectively, which correspond to the antisymmetric and symmetric stretching vibrations of the carbon skeleton of the benzene ring structure. In addition, because both complexes (II) and (III) are *meta*-disubstituted on the benzene ring, complex (II) absorbs out-of-plane bending vibrations of the C–H bond on the aromatic ring at 872 cm^{-1}, 795 cm^{-1}, and 715 cm^{-1} and complex (III) at 855 cm^{-1}, 790 cm^{-1}, and 712 cm^{-1}. As well as the benzene ring structure, there is an important sulfone group in the molecules of complexes (II) and (III), and an infrared absorption peak can be observed at 1297 cm^{-1} and 1300 cm^{-1}, respectively, corresponding to the asymmetric stretching vibration absorption peak of the S=O bond. At positions 1142 cm^{-1} and 1150 cm^{-1}, there are symmetric stretching vibrations of S=O in the two complex molecules, respectively. A strong absorption peak can be observed at 1045 cm^{-1} and 1092 cm^{-1}, which is the S=O stretching vibration characteristic infrared absorption peak of complexes (II) and (III) [27,28]. Although there are many similarities in the structures of complexes (II) and (III), there are also some differences. For example, the anions in complex molecules are not the same. Complex (II) contains NO_3^- ions in the molecule, and the strong stretching vibration peak range of the N–O bond of nitrate ions is generally between 1390 and 1370 cm^{-1}, as shown in the figure. Complex (II) shows a strong absorption peak at 1380 cm^{-1}, which proves that NO_3^- ions are indeed present in the molecule [29]. M-N exhibited a stretching vibration absorption peak in the range of 660–600 cm^{-1}, whereas M-O exhibited a stretching vibration absorption peak in the range of 600–500 cm^{-1}, indicating chelation between the metal and the ligand [30,31].

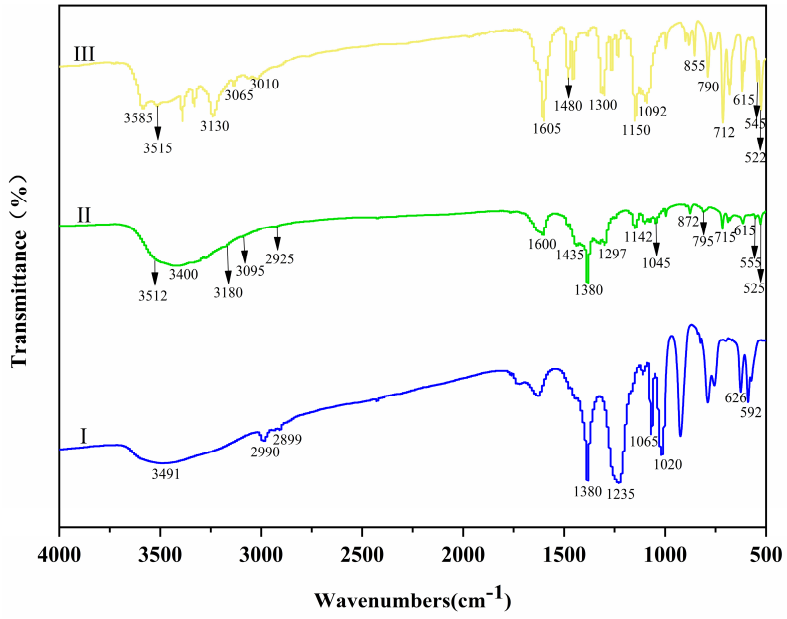


Figure 3. IR spectra of complexes (I) to (III) in the 4000–500 cm^{-1} region.

2.3. UV–Vis Spectral Analyses of Complexes (I)–(III)

The UV–visible spectra of complexes (I) and (III) at 200–800 nm are shown in Figure 4a,b shows the UV–visible spectra of complexes (I) and (II) at 300–1000 nm. Complex (I) has a weak absorption band at 260 nm, which is caused by the n → π* transition of the -S=O bond and belongs to the R absorption band. In addition, a wide absorption band at 810 nm can be observed in Figure 4b, which is caused by the d-d transition of Cu^{2+} with strong absorbance.

At 405 nm, a narrow absorption peak can be observed, which is caused by the d-d transition of Ni^{2+} with a lighter color and weaker absorbance [32]. The benzene rings in complexes (II) and (III) are both connected to the chromophore NH_2 and undergo n–π conjugation, causing both the E-band and the B-band of the benzene ring to redshift. Interestingly, the benzene rings in these two complexes are also replaced by the chromophore S=O. At this time, the double bond is conjugated with the benzene ring, and a K-band appears at 200–250 nm. The figure shows that complexes (II) and (III) have absorption bands at 228 nm and 230 nm, respectively. At the same time, the B-band of the benzene ring undergoes a significant redshift; that is, the B-band shifts from 255 nm to 315 nm.

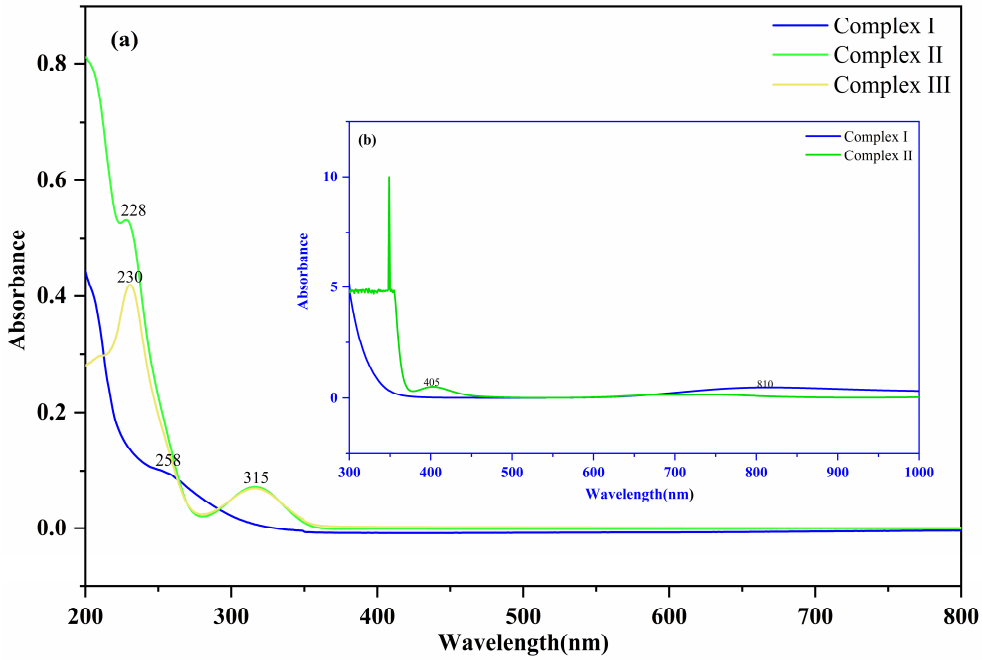


Figure 4. UV–Vis spectra of complexes (I)–(III) in the range of 200–1000 nm. ((**a**) shows the UV absorption spectra of complexes I–III at 200–800nm, while (**b**) shows the UV absorption spectra of complexes I–II at 300–1000 nm).

2.4. NMR Spectroscopy of Complex (III)

We also conducted ^{1}H NMR and ^{13}C NMR tests on complex (III), and Figure 5 shows the NMR spectra of this complex. The chemical shift of the hydrogen on the benzene ring is generally approximately 7.26 ppm [33]. In the figure, nuclear magnetic resonance signals can be observed at 7.08 ppm, 7.02 ppm, and 6.91 ppm, but the chemical shift is less than 7.26 ppm; this is most likely due to the substitution of the benzene ring with $-NH_2$ and $-SO_2$, which reduces the electron density on benzene carbons. The sulfone group is an electron-withdrawing group and has a deshielding effect on the hydrogen nucleus, resulting in an increase in the chemical shift value. The amino group is a strong electron-donating group, which increases the shielding effect when connected to the benzene ring, ultimately leading to a decrease in the chemical shift value. Due to the connection of two amino groups and one sulfone group in the molecule, the shielding effect is preserved. The nuclear magnetic resonance signal at δ = 5.20 ppm corresponds to the hydrogen atom on $-NH_2$. The chemical shift of amino hydrogen is influenced by neighboring functional groups, such as the conjugation and induction effects of benzene rings, as well as metal ions with low electronegativity. The ^{13}C NMR spectrum of complex (III) shows the presence of various types of carbon atoms in the complex, with chemical shift values of 112 ppm, 114 ppm, 118 ppm, 129 ppm, 142 ppm, and 149 ppm. The reason for the different chemical shift values is the same as that for the hydrogen spectrum and will not be elaborated on here.

The position on the benzene ring where the substituent is substituted has the largest change in chemical shift values, followed by the *ortho*- and *para*-positions, with the *meta*-carbon having the smallest impact [34].

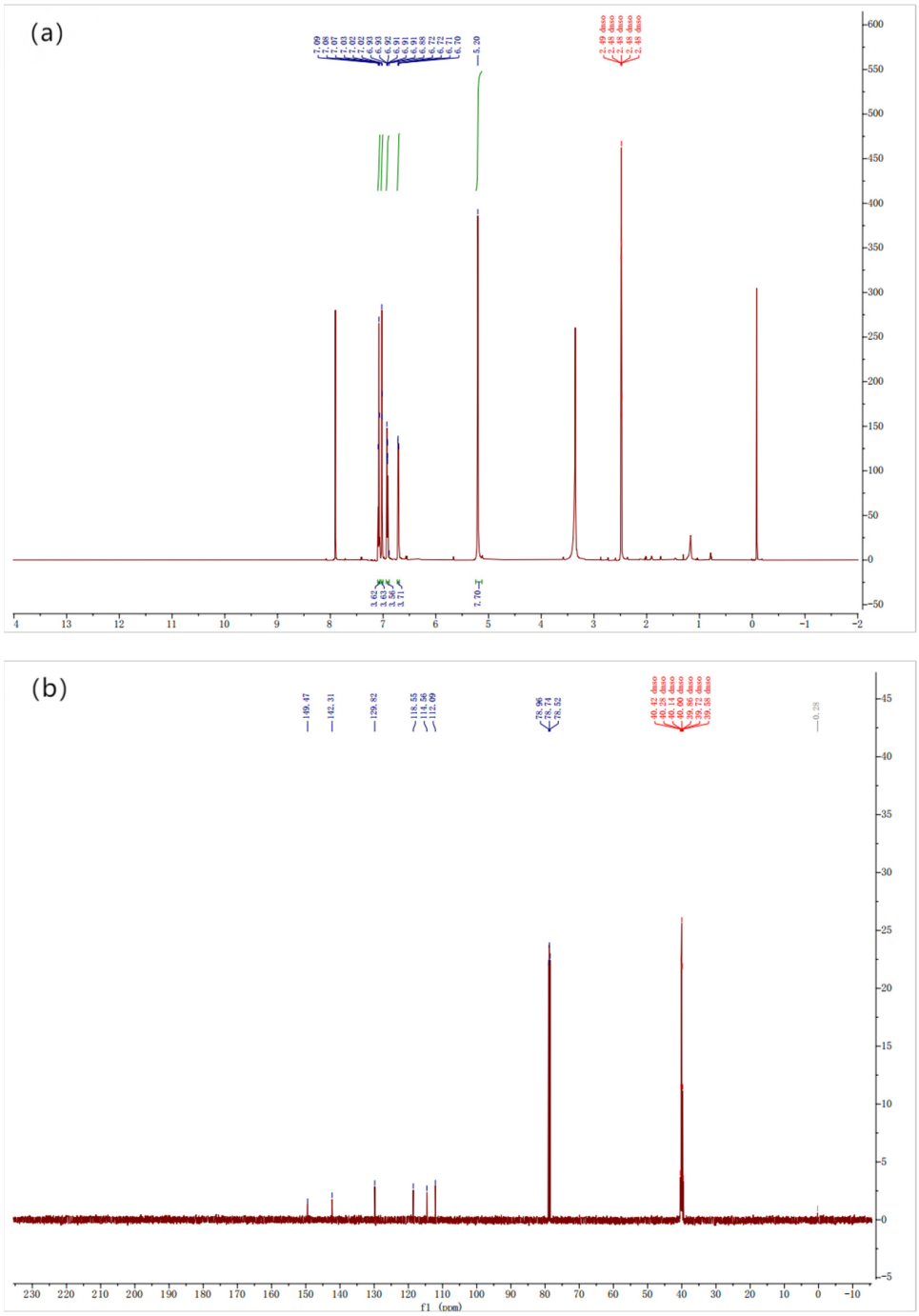


Figure 5. ^{1}H NMR (**a**) and ^{13}C NMR (**b**) spectra of complex (III).

2.5. Electrospray Mass Spectrum Analysis

The electrospray ionization mass spectrum peak of complexes (I)–(III) in ethanol solvent is shown in Figure 6, and the mass–charge (m/z) ratios are as follows: the molecular formula of complex (I) is [$C_4H_{18}CuO_{12}S_2$] (I), and the theoretical value of the mass–charge ratio is 384.84, while the actual value is 384.88 $[M+H]^+$. The molecular formula of complex (II) is [$C_{12}H_{18}N_4NiO_{11}S$] (II), and the theoretical value of the mass–charge ratio is 486.07, while the actual value is 485.92 $[M+H]^+$. The molecular formula of complex (III)

is $[C_{24}H_{24}Cl_2N_4O_4S_2Zn]$ (III), and the theoretical value of the mass–charge ratio is 631.86, while the actual value is 631.89 $[M-H]^+$.

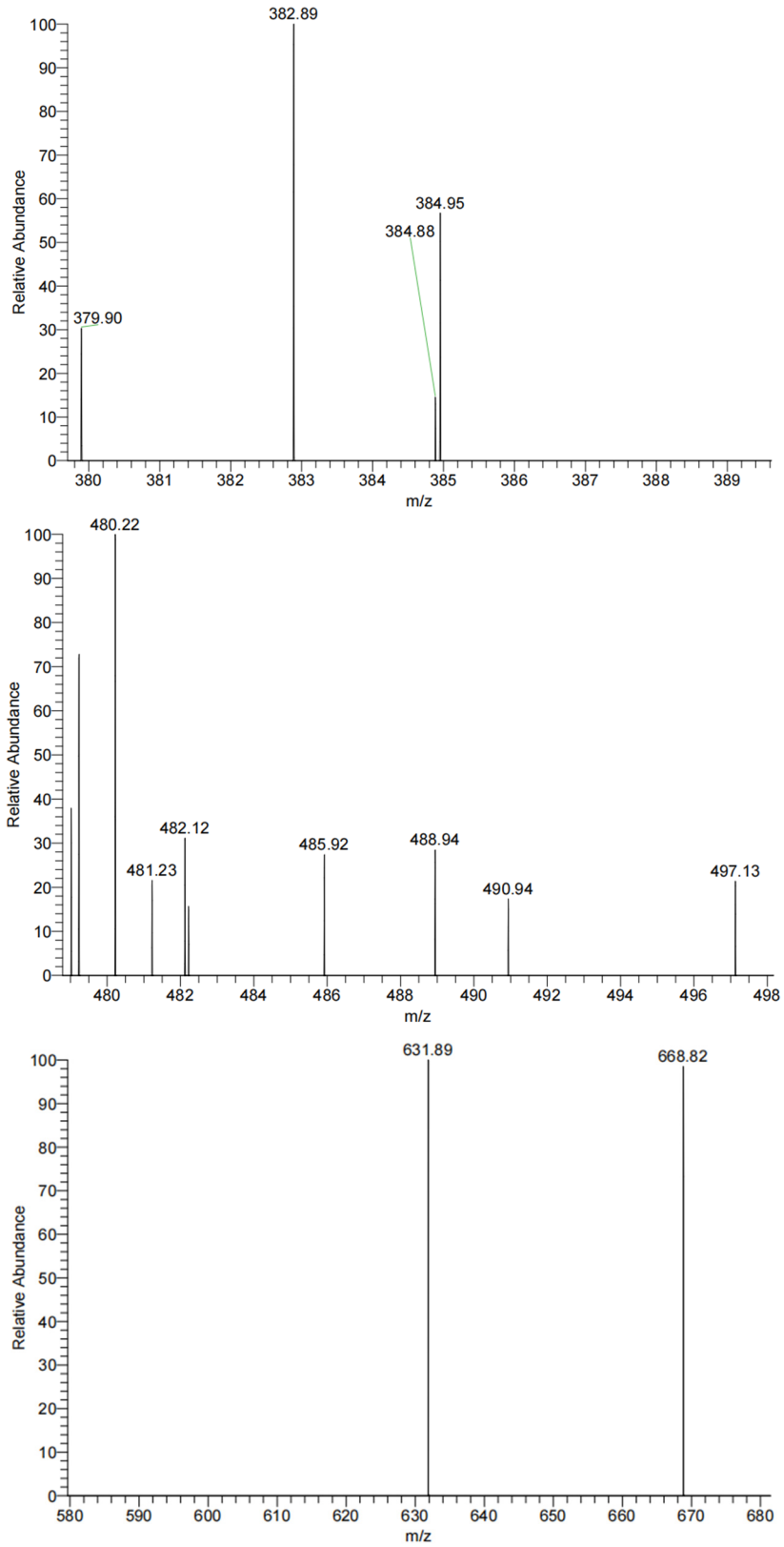


Figure 6. Electrospray ionization mass spectra of complexes (I)–(III).

2.6. Thermogravimetric Analysis for Complexes (I) to (III)

Thermogravimetric analysis (TGA) tests were conducted on complexes (I)–(III) within the temperature range of 30–900 °C, and the results are shown in Figure 7. The TGA curve of complex (I) shows four distinct stages of thermal decomposition. In the temperature range of 50–235 °C, complex (I) underwent continuous mass loss, and the first plateau appeared after this process, with mass losses of 2.68%, 40.91%, and 11.32%, respectively. These quality losses are mainly attributed to the decomposition of water molecules and ethyl sulfate ions in the complex. In the temperature range of 620–740 °C, the weight of complex (I) decreased again, and a second plateau period could be seen, with a mass loss of 17.98%. This stage of decomposition corresponds to the process of SO_4^{2-} in the complex decomposing into SO_3 gas. After these decomposition processes, the final remaining substance was CuO (calculated value: 20.48%, actual value: 19.23%). Complex (II) exhibited sustained weight loss in the temperature range of 35–535 °C, with a loss of 61.64% of the total mass, attributed to the decomposition of water molecules and ligands in the complex molecules. The final residual product was $Ni(NO_2)_2$ (calculated value: 30.92%, actual value: 30.63%). Complex (III) also underwent three distinct thermal decomposition processes, with the first stage occurring within the temperature range of 35–108 °C, resulting in a mass loss of 11.18%. This corresponds to the removal of two Cl^- ions from the complex molecules (calculated value: 11.22%). The temperature range of the second stage is 330–655 °C, with a total weight loss of 45.01%, which may correspond to the loss of two aniline molecules and two SO_2 molecules (calculated value: 50.33%).

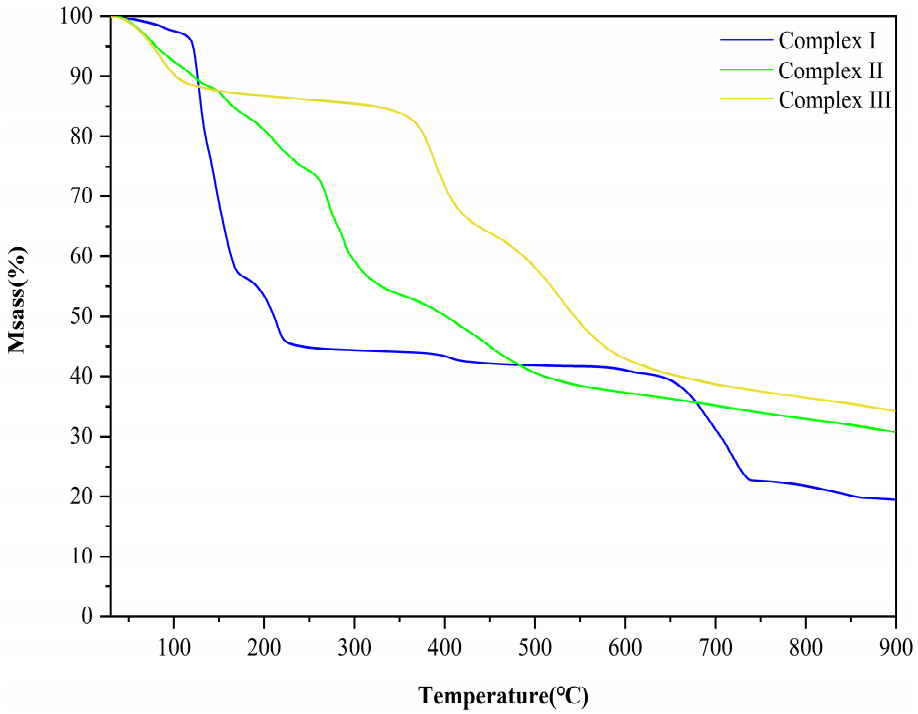


Figure 7. Thermogravimetric analysis (TGA) decomposition curves of complexes (I)–(III).

2.7. Cytotoxicity Assays of Complexes (I)–(III)

We conducted MTS cytotoxicity tests of complexes (I)–(III) against the human cancer cell lines lung cancer A549, liver cancer SMMC-7721, breast cancer MDA-MB-231, and colon cancer SW480 [35], and the results are shown in Table 2. The inhibition rates of complex (I) on two cancer cell lines, lung cancer A549 and liver cancer SMMC-7721, were tested. The table shows that the complex did not have a good inhibitory effect. In addition to complex (I), complexes (II) and (III) inhibited the cell growth of breast cancer cells MDA-MB-231 and

colon cancer cells SW480. The inhibition rates of the two complexes on MDA-MB-231 cells were relatively good, at (22.87 ± 1.52)% and (19.86 ± 1.20)%, respectively. The inhibition rates on the colon cancer cell line SW480 were (18.68 ± 0.44)% and (18.68 ± 0.89)%. In 2022, Kundalkesha D Gaikwad et al. synthesized a related complex using 4,4′-diaminodiphenyl sulfone and Co (II) and found that the complex exhibited significant inhibitory effects on the cancer cell line A549. This may be attributed to the fact that cobalt complexes can inhibit the activity of some key enzymes and proteins, effectively hindering the growth of cancer cells [36]. In contrast, nickel and zinc complexes have weaker effects on enzyme and protein inhibition, and their anti-cancer mechanisms are not rich or diverse enough. In addition, in the experimental results, complexes (I)–(III) did not exhibit good biological activity, which may be related to the insufficient stability of the complexes. The stability of metal–organic complexes in biological environments is one of the important factors affecting their biological activity. From the thermogravimetric curve (Figure 7), it can be observed that the structures of complexes (I)–(III) begin to change within the temperature range of 30–35 °C. The instability of this structure may be one of the reasons for the poor biological activity of the complexes. In the future research work of our laboratory, we will focus on studying the above-mentioned issues and increasing the thermal stability of the complex by adjusting its structure.

Table 2. Cancer cell inhibition rates of complexes (I)–(III).

Complex	A549		SMMC-7721		MDA-MB-231		SW480	
	Cell Inhibition (%)							
	Average	SD	Average	SD	Average	SD	Average	SD
I	10.49	0.74	7.86	1.87	-	-	-	-
II	15.51	0.37	6.86	0.76	22.87	1.52	18.68	0.44
III	15.88	0.90	3.52	0.90	19.89	1.20	18.68	0.89

3. Experimental

3.1. Materials and Methods

Bis(phenylacetyl) disulfide and 3,3′-diaminodiphenyl sulfone were purchased from Beijing Bailingwei Technology Co., Ltd. (Beijing, China), and the metal salt was purchased from China National Pharmaceutical Group Chemical Reagent Co., Ltd. (Shanghai, China). All of these drugs were of analytical purity and had undergone no further purification or separation operations. Elemental analysis of the complex was performed via a VARIO ELIII elemental analyzer (German Elemental Analysis Systems, Hanau, Germany). The crystal data were obtained using a Bruker D8 Venture four-circle single-crystal X-ray diffractometer (Oxford Diffraction, Oxford, England). The UV–visible absorption spectrum was recorded using a CARY 5000 UV–Vis near-infrared spectrophotometer (Agilent Technologies, Santa Clara, CA, USA), and the infrared spectrum was obtained using a Magna–IR 750 Fourier-transform infrared spectrometer (Thermo Nicolet Corporation, Waltham, MA, USA). ESI–MS and NMR data were obtained using a Vanquish Q Exactive Plus liquid chromatography quadrupole electrostatic field orbital trap mass spectrometer (Thermo Fisher Scientific, Waltham, MA, USA) and a 500 MHz Bruker Advance (III) spectrometer (Agilent Technologies, Santa Clara, CA, USA), respectively. The chemical shifts of the ^{1}H NMR and ^{13}C NMR data are expressed in ppm, with DMSO-d6 as the solvent and δ = 2.5 ppm. The thermogravimetric data were obtained with a NETZSCH TG209F1 thermal analyzer (PerkinElmer, Waltham, MA, USA) at a heating rate of 10 °C/min, with nitrogen gas used as the atmosphere during the experiment.

3.2. Synthesis of Complex (I)

Bis(phenylacetyl) disulfide (0.3020 g, 1 mmol) and $Cu(NO_3)_2 \cdot 3H_2O$ (0.4831 g, 2 mmol) were weighed separately and dissolved in 50 mL of anhydrous ethanol. The mixture was refluxed and stirred at 100 °C for 24 h and filtered while it was heated, and the obtained filtrate was slowly evaporated at room temperature. After approximately three days, the target complex (I) precipitated as blue columnar crystals. The samples were washed three times with petroleum ether and *n*-hexane, vacuum dried for 30 min, and weighed to 0.1526 g, and the yield was 39.6%, with an m.p. of 88.5–89.0 °C. Additional measurements were as follows: ESI-MS: 384.88 $[M-H]^+$; IR (KBr, υ, cm^{-1}): 3491(-O-H), 2990, 2899(-C-H), 1380 (-C-H), 1235 (-C-C), 1065, 1020 (-S=O), 626, 592 (-Cu-O). In $[C_4H_{18}CuO_{12}S_2]$(I) analysis, the calcd % values were as follows: S, 16.62; C, 12.44; H, 4.66. The found % values were as follows: S, 16.60; C, 12.83; H, 4.65.

We followed the above experimental method and reacted the ligand bis(phenylacetyl) disulfide with other metal salts ($Co(NO_3)_2 \cdot 6H_2O$, $Zn(NO_3)_2 \cdot 6H_2O$, $ZnCl_2$, and $Mn(CH_3COO)_2 \cdot 4H_2O$) at the same molar ratio, reaction temperature, and reaction time. The filtrate was filtered and allowed to evaporate naturally at room temperature. After approximately 1–2 days, white needle-shaped crystals precipitated from the filtrate, with a melting point of 112.0–114.3 °C.

3.3. Synthesis of Complex (II)

We weighed 3,3′-diaminodiphenyl sulfone (0.2482 g, 1 mmol) and $Ni(NO_3)_2 \cdot 6H_2O$ (0.5817 g, 2 mmol) at a molar ratio of 1:2 and dissolved them in 50 mL of anhydrous ethanol. The mixture was fixed at 100 °C for 24 h and then filtered. The filtrate was evaporated naturally at room temperature, and after a period of time, light green crystals of complex (II) were obtained. The mass was 0.3367 g, and the yield was 69.4%, with an m.p. of 103.6–104.5 °C. Additional measurements were as follows: ESI-MS: 485.92 $[M+H]^+$; IR (KBr, υ, cm^{-1}): 3512(-N-H), 3400(-O-H), 3180, 3095, 2925 (-C-H), 1600, 1435(-C=C), 872, 795, 715 (-C-H), 1297, 1142, 1045 (-S=O), 1380 (-N-O), 615(-Ni-O), 555, 525 (-Ni-N). In $[C_{12}H_{18}N_4NiO_{11}S]$(II) element analysis, the calcd % values were as follows: N, 11.54; C, 29.68; H, 3.710. The found % values were as follows: N, 11.84; C, 29.25; H, 3.971.

3.4. Synthesis of Complex (III)

The synthesis methods used for complexes (II) and (III) are essentially the same; that is, 3,3′-diaminodiphenyl sulfone (0.2482 g, 1 mmol) and $ZnCl_2$ (0.2726 g, 2 mmol) were precisely weighed and dissolved in 50 mL anhydrous ethanol. The mixture was refluxed at 100 °C for 24 h and then hot-filtered. The filtrate was evaporated naturally at room temperature. After a period of time, a light brown complex (III) was obtained with a mass of 0.2645 g and a yield of 83.6%, with an m.p. of 269.0–270.0 °C. Additional measurements were as follows: ESI-MS: 631.89 $[M-H]^+$; IR (KBr,υ, cm^{-1}): 3585, 3515(-N-H), 3130, 3065, 3010 (-C-H), 1605, 1480(-C=C), 855, 790, 712 (-C-H), 1300, 1150, 1092 (-S=O), 615(-Zn-O), 545, 522 (-Zn-N). In $[C_{24}H_{24}Cl_2N_4O_4S_2Zn]$(III) element analysis, the calcd % values were as follows: N, 8.85; C, 45.51; H, 3.79. The found % values were as follows: N, 8.97; C, 45.75; H, 4.07.

3.5. X-Ray Structure

The crystal data of complexes (I)–(III) were collected using a Bruker D8 Venture type four-circle single-crystal X-ray diffractometer at room temperature via GaK α (λ = 1.34139 Å) rays. The programs SHELXT [37] and SHELXL-2018/3 [38] were used to determine and refine the structure of the complex. To facilitate the analysis of the crystal structure, anisotropic refinement was performed on nonhydrogen atoms in the complex molecules,

whereas constrained isotropic refinement was performed on hydrogen atoms, omitting hydrogen atoms in the complex. The crystal data, typical bond lengths, and bond angles of the complexes are shown in Tables 1 and 3.

Table 3. Crystal data and refinement parameters for compounds (I)–(III).

Complex	I		II	III
Empirical formula	$C_4\ H_{18}CuO_{12}S_2$	S_8	$C_{12}\ H_{18}\ N_4\ Ni\ O_{11}\ S$	$C_{24}\ H_{24}\ Cl_2\ N_4\ O_4\ S_2\ Zn$
Formula weight	385.84	256.48	485.07	632.86
Temperature	200(2) K	200(1) K	102(2) K	200(2) K
Wavelength	1.34139	1.34139	1.34139	1.34139
Crystal system	Orthorhombic	Orthorhombic	Monoclinic	Monoclinic
Space group	Pbca	Fddd	$P2_1/n$	P2/n
a/Å	9.7657(8)	10.4397(12)	12.7468(6)	12.0055(7)
b/Å	7.3279(7)	12.8489(12)	7.6955(4)	5.0078(3)
c/Å	19.7608(17)	24.482(3)	19.1076(12)	22.2135(14)
α/°	90	90	90	90
β/°	90	90	104.886(2)	98.700(2)
γ/°	90	90	90	90
Volume	1414.6(2)	3284.0(6)	1811.42(17)	1320.13(14)
Z	4	16	4	2
D_{calcd} g/cm^3	1.812	2.075	1.779	1.592
μ (mm^{-1})	10.521	12.841	6.977	3.288
F(000)	796	2048	1000	648
2θ range (°)	11.08–144.54	10.004–103.808	3.277–61.972	3.442–56.749
Reflections collected	17,501	1176	25,756	16,456
Independent reflections	2104	529	25,756	2615
Final R indices [I >= 2σ(I)]	R1 = 0.0291, wR2 = 0.843	R1 = 0.1015, wR2 = 0.2766	R1 = 0.0663, wR2 = 0.1605	R1 = 0.0354,wR2 = 0.0993
Final R indices [all data]	R1 = 0.0321, wR2 = 0.0870	R1 = 0.1295, wR2 = 0.3736	R1 = 0.0913, wR2 = 0.1708	R1 = 0.0450, wR2 = 0.1030

3.6. Cytotoxicity Assay

The A549, SMMC-7721, MDA-MB-231, and SW480 cancer cell lines used in the experiment were all obtained from ATCC (Manassas, VA, USA). The cells were cultivated and inoculated with 10% fetal bovine serum culture medium at 37 °C. The MTS method was used to detect cell viability in the experiment [39]. The principle involves the use of succinate dehydrogenase in the mitochondria of cells to reduce the MTS and generate soluble formazan compounds. The number of formazan compounds produced was used to estimate the number of live cells.

4. Conclusions

In this work, two sulfur-containing ligands were directly reacted with $Cu(NO_3)_2{\cdot}3H_2O$, $Ni(NO_3)_2{\cdot}6H_2O$, and $ZnCl_2$ to synthesize three types of complex crystals: $[C_4H_{18}CuO_{12}S_2]$(I), $[C_{12}H_{18}N_4NiO_{11}S]$(II), and $[C_{24}H_{24}Cl_2N_4O_4S_2Zn]$(III). The structure of the complex was characterized and analyzed using modern analytical techniques, such as EA, XRD, FT-IR, UV, NMR, ESI-MS, and TGA, and the cytotoxicity of the complex crystals was preliminarily studied. Complexes (I)–(III) were initially screened for cytotoxicity using the MTS method to explore their potential as anticancer agents. The experimental data showed that complex (II) had a relatively good inhibitory effect on breast cancer MDA-MB-231. A simpler experimental method for preparing elemental sulfur was also discovered during the experiment. At present, the laboratory is still improving the experimental protocol by optimizing the ligand structure, selecting the appropriate metal center, and improving the synthesis method, with the expected results of improved cytotoxicity synthesis, better selectivity, and fewer toxic side effects in the future.

Author Contributions: Y.Y.: Writing—original draft, validation, investigation, data curation, conceptualization, visualization, and writing—original draft. D.L.: Assisted in completing the experiments. M.L.: Writing—review and editing, writing—original draft, visualization, validation, supervision, software, and resources. All authors have read and agreed to the published version of the manuscript.

Funding: This work was supported by Hefei University of Technology and the State Key Laboratory of Photochemistry and Plant Resources of West China.

Data Availability Statement: CCDC: 2385433(I), 2385441(II), and 2385435(III) supplementary crystallographic data were utilized for this study. These data are available free of charge from the Cambridge Crystallography Data Centre via www.ccdc.cam.ac.uk/data_request/cif (accessed on 20 September 2024).

Conflicts of Interest: The authors declare that they have no known competing financial interests or personal relationships that could have appeared to influence the work reported in this paper.

References

1. Aziz, K.N.; Ahmed, K.M.; Omer, R.A.; Qader, A.F.; Abdulkareem, E.I. Organometallic complexes and reaction methods for synthesis: A review. *Rev. Inorg. Chem.* **2024**, *44*, 685–698. [CrossRef]
2. Abdolmaleki, S.; Khaksar, S.; Aliabadi, A.; Panjehpour, A.; Motieiyan, E.; Marabello, D.; Faraji, M.H.; Beihaghi, M. Cytotoxicity and mechanism of action of metal complexes: An overview. *Toxicology* **2023**, *492*, 153516. [CrossRef]
3. Marakina, E.I.; Andrienko, O.S.; Sachkov, V.I.; Medvedev, R.; Amelichkin, I.; Shcherbakov, P.S. Transition metals in the process of complexation with organic ligands containing heteroatoms in the structure. *J. Phys. Conf. Ser.* **2021**, *1989*, 012027. [CrossRef]
4. Wu, Y.; Wu, T.; Huang, Y. A review: Biological activities of novel cyanopyridine derivatives. *Arch. Pharm.* **2023**, *356*, 2300067. [CrossRef] [PubMed]
5. Mendez-Arriaga, J.M. Recent advances in biological and catalytic applications of metal complexes. *Inorganics* **2024**, *12*, 249. [CrossRef]
6. Liu, X.; Manzur, C.; Novoa, N.; Celedón, S.; Carrillo, D.; Hamon, J.R. Multidentate unsymmetrically-substituted Schiff bases and their metal complexes: Synthesis, functional materials properties, and applications to catalysis. *Coord. Chem. Rev.* **2018**, *357*, 144–172. [CrossRef]
7. Ndagi, U.; Mhlongo, N.; Soliman, M.E. Metal complexes in cancer therapy—An update from drug design perspective. *Drug Des. Dev. Ther.* **2017**, *11*, 599–616. [CrossRef] [PubMed]
8. Lee, L.C.C.; Lo, K.K.W. Shining new light on biological systems: Luminescent transition metal complexes for bioimaging and biosensing applications. *Chem. Rev.* **2024**, *124*, 8825–9014. [CrossRef] [PubMed]
9. Li, D.; Shi, W.J.; Hou, L. Coordination polymers of copper(I) halides and neutral heterocyclic thiones with new coordination modes. *Inorg. Chem.* **2005**, *44*, 3907–3913. [CrossRef]
10. Pósa, V.; Hajdu, B.; Tóth, G.; Dömötör, O.; Kowol, C.R.; Keppler, B.K.; Spengler, G.; Gyurcsik, B.; Enyedy, É.A. The coordination modes of (thio)semicarbazone copper(II) complexes strongly modulate the solution chemical properties and mechanism of anticancer activity. *J. Inorg. Biochem.* **2022**, *231*, 111786. [CrossRef]
11. Cascajosa-Lira, A.; Andreo-Martínez, P.; Prieto, A.I.; Baños, A.; Guillamón, E.; Jos, A.; Cameán, A.M. In vitro toxicity studies of bioactive organosulfur compounds from Allium spp. with potential application in the agri-food industry: A review. *Foods* **2022**, *11*, 2620. [CrossRef] [PubMed]
12. Petropoulos, S.; Di Gioia, F.; Ntatsi, G. Vegetable organosulfur compounds and their health promoting effects. *Curr. Pharm. Des.* **2017**, *23*, 2850–2875. [CrossRef]
13. Bhattacherjee, D.; Raina, K.; Mandal, T.K.; Thummer, R.P.; Bhabak, K.P. Targeting Wnt/β-catenin signaling pathway in triple-negative breast cancer by benzylic organotrisulfides: Contribution of the released hydrogen sulfide towards potent anti-cancer activity. *Free Radic. Biol. Med.* **2022**, *191*, 82–96. [CrossRef] [PubMed]
14. Shoaib, S.; Ansari, M.A.; Ghazwani, M.; Hani, U.; Jamous, Y.F.; Alali, Z.; Wahab, S.; Ahmad, W.; Weir, S.A.; Alomary, M.N.; et al. Prospective epigenetic actions of organo-sulfur compounds against cancer: Perspectives and molecular mechanisms. *Cancers* **2023**, *15*, 697. [CrossRef]
15. Samaei, N.M.; Yazdani, Y.; Alizadeh-Navaei, R.; Azadeh, H.; Farazmandfar, T. Promoter methylation analysis of WNT/β-catenin pathway regulators and its association with expression of DNMT1 enzyme in colorectal cancer. *J. Biomed. Sci.* **2014**, *21*, 73. [CrossRef]
16. Debnath, T.; Deb Nath, N.C.; Kim, E.K.; Lee, K.G. Role of phytochemicals in the modulation of miRNA expression in cancer. *Food Funct.* **2017**, *8*, 3432–3442. [CrossRef]
17. Soltani, S.; Amin, G.R.; Salehi-Sourmaghi, M.H.; Schneider, B.; Lorenz, S.; Iranshahi, M. Sulfur-containing compounds from the roots of Ferula latisecta and their cytotoxic activities. *Fitoterapia* **2018**, *124*, 108–112. [CrossRef]
18. Balakrishnan, S.; Duraisamy, S.; Kasi, M.; Kandasamy, S.; Sarkar, R.; Kumarasamy, A. Syntheses, physicochemical characterization, antibacterial studies on potassium morpholine dithiocarbamate nickel (II), copper (II) metal complexes and their ligands. *Heliyon* **2019**, *5*, e01687. [CrossRef]

19. Yekke-Ghasemi, Z.; Ramezani, M.; Mague, J.T.; Takjoo, R. Synthesis, characterization and bioactivity studies of new dithiocarbazate complexes. *New J. Chem.* **2020**, *44*, 8878–8889. [CrossRef]
20. Singh, A.; Barman, P.; Gogoi, H.P. Thioether-based novel transition metal complexes: Synthesis, DNA interaction, in vitro biological assay, DFT calculations, and molecular docking studies. *Bioorg. Chem.* **2023**, *132*, 106343. [CrossRef] [PubMed]
21. Czylkowska, A.; Pitucha, M.; Lanka, S.; Raducka, A.; Rogalewicz, B.; Szczesio, M.; Świątkowski, M.; Żarczyński, A.; Klepacz-Smółka, A.; Szczytko, J.; et al. Triazole-based Mn(II), Fe(II), Ni(II), Cu(II) and Zn(II) complexes as potential anticancer agents—Physicochemical properties, in silico predictions and in vitro activity. *Polyhedron* **2024**, *261*, 117106. [CrossRef]
22. Luo, M.; Zhang, J.C.; Yin, H.; Wang, C.M.; Morris-Natschke, S.; Lee, K.H. One-step templated synthesis of chiral organometallic salicyloxazoline complexes. *BMC Chem.* **2019**, *13*, 51. [CrossRef]
23. Kim, G.; Na, C.W.; Myung, Y. Facile one-pot synthesis of nickel nanoparticles by hydrothermal method. *Materials* **2022**, *16*, 76. [CrossRef]
24. Cepus, V.; Borth, M.; Seitz, M. IR spectroscopic characterization of lignite as a tool to predict the product range of catalytic decomposition. *Int. J. Clean Coal Energy* **2016**, *5*, 13–22. [CrossRef]
25. İlkimen, H.; Salün, S.G.; Gülbandılar, A.; Sarı, M. The new salt of 2-amino-3-methylpyridine with dipicolinic acid and its metal complexes: Synthesis, characterization and antimicrobial activity studies. *J. Mol. Struct.* **2022**, *1270*, 133961. [CrossRef]
26. Wang, Y.; Mao, X.; Chen, C.; Wang, W.; Dang, W. Effect of sulfuric acid concentration on morphology of calcium sulfate hemihydrate crystals. *Mater. Res. Express* **2020**, *7*, 105501. [CrossRef]
27. Yadav, V.; Niluroutu, N.; Bhat, S.D.; Kulshrestha, V. Sulfonated poly(ether sulfone) based sulfonated molybdenum sulfide composite membranes: Proton transport properties and direct methanol fuel cell performance. *Mater. Adv.* **2020**, *1*, 820–829. [CrossRef]
28. Mabrouk, W.; Charradi, K.; Maghraoui-Meherzi, H.; Alhussein, A.; Keshk, S.M.A.S. Proton conductivity amelioration of sulfonated poly ether sulfone octyl sulfonamide via the incorporation of montmorillonite. *J. Electron. Mater.* **2022**, *51*, 6369–6378. [CrossRef]
29. Kumar, D.; Kapoor, I.P.S.; Singh, G.; Fröhlich, R. Preparation, characterization, and kinetics of thermolysis of nickel and copper nitrate complexes with 2,2′-bipyridine ligand. *Thermochim. Acta* **2012**, *545*, 67–74. [CrossRef]
30. Sakthivel, R.V.; Sankudevan, P.; Vennila, P.; Venkatesh, G.; Kaya, S.; Serdaroğlu, G. Experimental and theoretical analysis of molecular structure, vibrational spectra and biological properties of the new Co(II), Ni(II) and Cu(II) Schiff base metal complexes. *J. Mol. Struct.* **2021**, *1233*, 130097. [CrossRef]
31. Aravindan, P.; Sivaraj, K.; Kamal, C.; Vennila, P.; Venkatesh, G. Synthesis, molecular structure, spectral characterization, molecular docking and biological activities of (E)-N-(2-methoxy benzylidene) anthracene-2-amine and Co(II), Cu(II) and Zn(II) complexes. *J. Mol. Struct.* **2021**, *1229*, 129488. [CrossRef]
32. Yu, T.; Zhu, Z.; Bao, Y.; Zhao, Y.; Liu, X.; Zhang, H. Investigation of novel carbazole-functionalized coumarin derivatives as organic luminescent materials. *Dyes Pigments* **2017**, *147*, 260–269. [CrossRef]
33. Gaikwad, K.D.; Ubale, P.; Khobragade, R.; Deodware, S.; Dhale, P.; Asabe, M.R.; Ovhal, R.M.; Singh, P.; Vishwanath, P.; Shivamallu, C.; et al. Preparation, characterization and in vitro biological activities of new diphenylsulphone derived schiff base ligands and their Co(II) complexes. *Molecules* **2022**, *27*, 8576. [CrossRef] [PubMed]
34. Chen, L.; Tan, J.; Lan, T.; Huo, H.; Sun, L.; Jiang, Y.; Zhang, N.; Li, C.; Wang, J. Effect of ligand structure on ethylene oligomerization over salicylaldehyde imine nickel complexes: Experiments and calculations. *Appl. Organomet. Chem.* **2023**, *37*, e7276. [CrossRef]
35. Mosbah, H.K.; Ibrahim, A.B.M.; Zidan, A.S.A.; Aly, A.A.M.; Saber, S.H. La(III), Ce(III), Pr(III) and Eu(III) complexes with fenamic acid based ligands: Preparation, spectral and thermal analysis and evaluation of their cytotoxicity in MDA-MB-231 breast cancer cells. *J. Iran. Chem. Soc.* **2024**, *21*, 1681–1689. [CrossRef]
36. Ambika, S.; Manojkumar, Y.; Arunachalam, S.; Gowdhami, B.; Sundaram, K.K.M.; Solomon, R.V.; Venuvanalingam, P.; Akbarsha, M.A.; Sundararaman, M. Biomolecular Interaction, Anti-Cancer and Anti-Angiogenic Properties of Cobalt(III) Schiff Base Complexes. *Sci. Rep.* **2019**, *9*, 2721. [CrossRef] [PubMed]
37. Amer, A.A. Synthesis of some new polyfunctionalized pyridines. *J. Heterocycl. Chem.* **2017**, *55*, 297–301. [CrossRef]
38. Dyachenko, I.V.; Dyachenko, V.D.; Dorovatovsky, P.V.; Khrustalev, V.N.; Nenajdenko, V.G. One-pot synthesis of thieno[2,3-b]pyridine and pyrido[3′,2′:4,5]thieno[3,2-d]pyrimidine derivatives. *Russ. J. Org. Chem.* **2020**, *56*, 974–982. [CrossRef]
39. Zhang, L.; Yin, H.; Zhang, J.C.; Luo, M.; Meng, X.G. Synthesis, crystal structure and anticancer activity of 4-chloro-2-methoxybenzoic acid transition metal complexes. *J. Mol. Struct.* **2024**, *1316*, 139080. [CrossRef]

Disclaimer/Publisher's Note: The statements, opinions and data contained in all publications are solely those of the individual author(s) and contributor(s) and not of MDPI and/or the editor(s). MDPI and/or the editor(s) disclaim responsibility for any injury to people or property resulting from any ideas, methods, instructions or products referred to in the content.